Kondo resonance in a magnetically ordered compound Ce_2RhSi_3: Photoemission spectroscopy and *ab initio* band structure calculations

Swapnil Patil, V. R. R. Medicherla, R. S. Singh, Sudhir K. Pandey, E. V. Sampathkumaran, and Kalobaran Maiti*
Department of Condensed Matter Physics and Materials Science, Tata Institute of Fundamental Research, Homi Bhabha Road, Colaba, Mumbai 400005, India

(Received 19 August 2010; revised manuscript received 27 August 2010; published 24 September 2010)

We study the electronic structure of an antiferromagnetic metal, Ce_2RhSi_3 ($T_N<7$ K), using high-resolution photoemission spectroscopy and *ab initio* band structure calculations. The valence-band spectra at higher binding energies are well described within the local-density approximations. The high-resolution spectra near Fermi level reveals the emergence of the Kondo resonance features with the decrease in temperature, which are distinctly different from the features appearing due to magnetic Ce $4f$ contributions. These results provide a direct evidence that the Kondo compensation effect of the local moments persists in this magnetically ordered compound, thereby, supporting the validity of the ideas based on spin-density-wave state as quantum criticality is approached.

DOI: 10.1103/PhysRevB.82.104428 PACS number(s): 75.20.Hr, 71.15.Mb, 71.27.+a, 71.28.+d

I. INTRODUCTION

Ce intermetallics have attracted great deal of attention in the scientific community due to the finding of various unusual ground states such as valence fluctuations, Kondo screening, heavy-fermion superconductivity, etc., due to the strong hybridization of the Ce $4f$ states with the conduction electronic states.[1] Such hybridization leads to the Kondo effect, which is characterized by the logarithmic enhancement of the electrical resistivity with reducing temperature. Further reduction in temperature leads to the formation of Kondo singlet (nonmagnetic) state, which is manifested as a sharp feature (Kondo resonance) at the Fermi level, ϵ_F. On the other hand, the valence electrons also mediate intersite exchange interaction among Ce $4f$ moments. The ground state of these systems depends on the balance between the indirect exchange interaction and Kondo coupling strengths. If the coupling strength is weak, long-range magnetic order is observed. Nonmagnetic phase appears in the strong-coupling limit. Thus, a change in the coupling strength leads the system from a long-range-ordered phase to a nonmagnetic phase via quantum critical point (QCP), where the quantum fluctuations are dominant.[2] An important issue widely discussed is the understanding of the approach to quantum criticality.[3,4] There are two school of thoughts at present: (i) local quantum criticality, where Kondo temperature, T_K goes to zero as one approaches the quantum critical point[5] and (ii) spin-density-wave (SDW) quantum criticality, where highly correlated $4f$ electrons leading to magnetic order also possess itineracy due to Kondo resonance formation ($T_K>0$ at the QCP).[6]

In this paper, we have studied an intermetallic compound, Ce_2RhSi_3, using state-of-the-art high-resolution photoemission spectroscopy. Ce_2RhSi_3 forms in AlB_2 structure and is antiferromagnetic at low temperature, $T_N<7$ K.[7–11] Various studies involving lattice compression/expansion via external pressure or chemical substitutions at the Ce and Si sites suggested that this compound lies close to the peak of Doniach's magnetic phase diagram.[12] Thus, this is well suited to investigate the persistence of Kondo compensation effect in a magnetically ordered phase. Our high-resolution photoemission data reveals sharp and distinct features near ϵ_F. The intensity of this feature exhibits temperature dependence confirming their link to Kondo singlet formation that supports the validity of SDW scenario in this case.

II. EXPERIMENTAL DETAILS

The sample, Ce_2RhSi_3 was prepared in the polycrystalline form by arc-melting of stoichiometric amounts of constituent elements in an atmosphere of high-purity argon. The molten ingots were subsequently homogenized in vacuum at 800 °C for 5 days. X-ray diffraction patterns using Cu $K\alpha$ line reveal that the sample formed in single phase; the crystal structure is AlB2-derived hexagonal structure. Magnetic-susceptibility measurements in the temperature range of 1.8–300 K in the presence of a magnetic field of 5 kOe were performed employing a commercial vibrating sample magnetometer (Oxford Instruments, U.K.). The experimental results exhibit onset of antiferromagnetic order at a temperature of about 7 K.[7]

The photoemission measurements were carried out using Gammadata Scienta electron analyzer, SES2002 and monochromatic photon sources at a base pressure of 3×10^{-11} torr. The energy resolutions were set to 0.4 eV, 5 meV, and 5 meV at Al $K\alpha$ (1486.6 eV), He II (40.8 eV), and He I (21.2 eV) photon energies, respectively. The sample surface was cleaned by *in situ* scraping using a diamond file and the surface cleanliness was ensured by the absence of O $1s$ and C $1s$ signals. The temperature variation was achieved using an open cycle helium cryostat, LT-3M from Advanced Research Systems, USA. The reproducibility of the spectra was ensured after each trial of scrapping. The Fermi level was determined at each temperature by measuring the Fermi cutoff in the spectral function of high-purity silver mounted in electrical contact with the sample.

III. CALCULATIONAL DETAILS

The electronic band structure calculations were carried out considering 512 k points within the first Brillouin zone

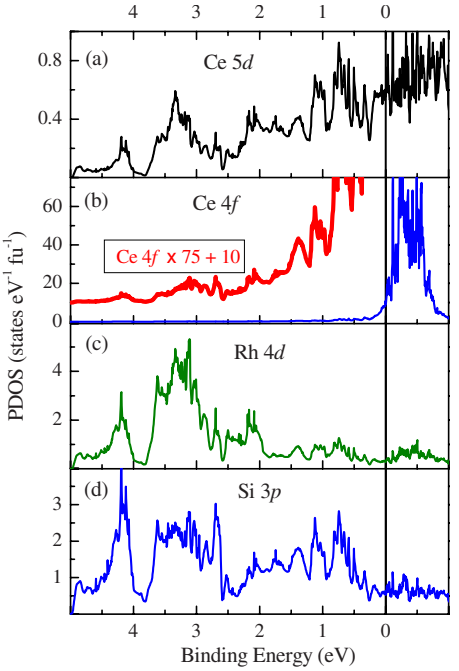

FIG. 1. (Color online) Calculated (a) Ce 5*d* PDOS, (b) Ce 4*f* PDOS, (c) Rh 4*d* PDOS, and (d) Si 3*p* PDOS. (Ce 4*f* PDOS × 75 +10) is shown by thick line in (b) for clarity in the higher binding energy region.

using *state-of-the-art* full-potential linearized augmented plane-wave method within the local-density approximations (WIEN2K software).[13] The lattice parameters were taken from the published literature.[7] The muffin-tin radii for Ce, Rh, and Si were set to 2.5 a.u., 2.2 a.u., and 1.95 a.u., respectively. The error bar for the energy convergence was set to <0.2 meV/f.u. In every case, the charge convergence was achieved to be less than 10^{-3} electronic charge.

IV. RESULTS AND DISCUSSIONS

The calculated partial density of states (PDOS) are shown in Fig. 1. The major contributions in this energy range arise from Ce 4*f*, Rh 4*d*, and Si 3*p* PDOS as shown in Figs. 1(b)–1(d), respectively. The Ce 5*d* contributions are small [see Fig. 1(a)] and almost equally distributed over the whole energy range shown. Rh 4*d* and Si 3*p* electronic states are found to be strongly hybridized. The bonding states[14,15] appear at binding energies ≥ 2 eV and possess dominant Rh 4*d* character while the antibonding features appear in the energy range of 0.5–2 eV having dominant Si 3*p* contributions. Ce 4*f* band is intense, narrow, and appear essentially above ϵ_F. The occupied part of Ce 4*f* appears within about 1 eV of ϵ_F. To investigate the contributions at higher binding energies, we have multiplied Ce 4*f* PDOS by 75 and shifted as shown by thick solid line in Fig. 1(b). Evidently, the distribution of PDOS at higher binding energies follows the behavior similar to that found in Rh 4*d* and Si 3*p*. This suggests that Ce 4*f* has finite hybridization with the electronic states having both Rh 4*d* character and Si 3*p* character.

Clearly, the major contributions in the valence band come from Ce 4*f*, Rh 4*d*, and Si 3*p* PDOS. Since the transition

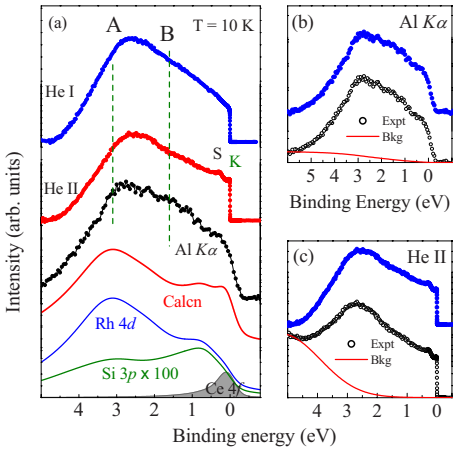

FIG. 2. (Color online) (a) Valence-band spectra collected at 10 K using He I, He II, and Al $K\alpha$ excitation energies. The calculated Al $K\alpha$ spectrum from the *ab initio* results are also shown along with the relative contributions from Rh 4*d*, Si 3*p*, and Ce 4*f* electronic states. The background subtraction procedure for two representative cases (b) Al $K\alpha$ and (c) He II spectra are also shown. The open symbols are the raw data, line is the background, and solid symbols are the background subtracted data.

probability of the photoelectrons in the photoexcitation process strongly depends on the excitation energies (matrix-element effect), a comparison of the photoemission spectra collected at different excitation energies would help to identify experimentally the character of various features constituting the valence band. In Fig. 2(a), we show the valence-band spectra collected at 10 K using Al $K\alpha$, He II, and He I photon energies after suitable background subtraction as shown in the Figs. 2(b) and 2(c).[16] The background function in the binding energy region, 0–3 eV, is significantly weak and hence has negligible influence on spectral intensities.

All the spectra exhibit a peak, A, centered at about 2.6 eV and with gradually decreasing intensities toward ϵ_F. The intensity near ϵ_F increases with the increase in photon energy. In addition, He II spectrum exhibits two distinct features S and K, which are not visible in the He I spectrum although the energy resolution in both these cases is identical. The photoemission cross section for Ce 4*f* states at He II excitation energy is about three times larger than that at He I photon energy while it is almost the same for Si 3*p* and Rh 4*d* states.[17] Thus, the features S and K in the He II spectrum can be attributed to the photoemission signal from the Ce 4*f* states. The high-energy resolution employed in the He I and He II measurements made it possible to resolve the distinct signatures of these features.

We have calculated the Al $K\alpha$ spectrum in the following way: the Ce 5*d*, Ce 4*f*, Rh 4*d*, and Si 3*p* PDOS per formula unit were multiplied by the corresponding photoemission cross sections at Al $K\alpha$ energy. The sum of all these contributions was convoluted by the Fermi distribution function at 10 K and broadened by a Lorentzian accounting the photohole lifetime broadening. The resolution broadening is introduced via Gaussian convolution [full width at half maximum (FWHM=0.4 eV)]. The calculated spectrum is shown in Fig. 2(a). The feature, A, dominated by the Rh 4*d* states is

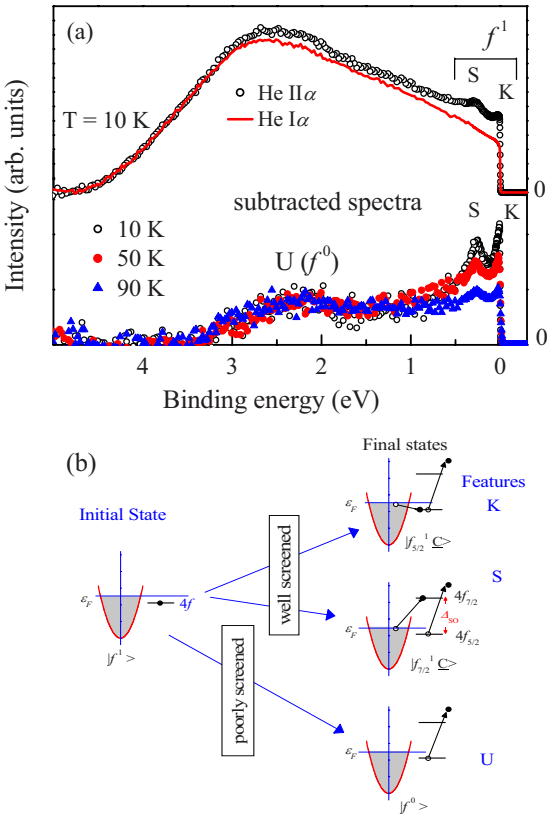

FIG. 3. (Color online) (a) He II (symbols) and He I (line) spectra at 10 K. The subtracted (He II-He I) spectra at different temperatures are shown in the bottom panel. (b) Schematic description of possible final states corresponding to the Ce 4*f* photoemission having $|f^1\rangle$ initial-state configuration.

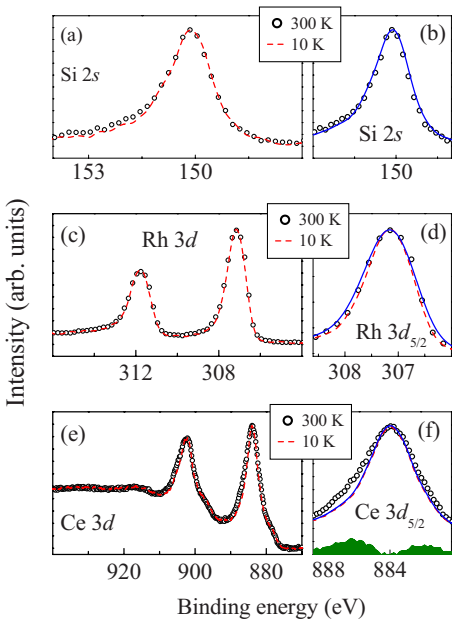

FIG. 4. (Color online) Core-level spectra at 300 K (symbols) and 10 K (dashed line). The 10 K spectra is broadened by a Gaussian and shown by solid line. The solid and dashed lines in (f) for Ce $3d_{5/2}$ feature are identical.

well reproduced by the calculated spectrum. The Ce 4*f* states contribute in the near ϵ_F region. The intensity around B in Fig. 2(a) is somewhat underestimated in the calculated spectrum although the energy position of various features are well captured. This discrepancy in intensity could be due to inaccurate accounting of matrix element effects[18] and/or final-state effects not considered in the band structure calculations. It is, however, clear that consideration of electron correlation among Rh 4*d* electrons may not be necessary to derive the electronic structure of this system as electron correlation usually generate features at higher binding energies,[19] which are not present in the experimental spectrum.

It is now established that the features near ϵ_F are primarily related to the Ce 4*f* photoemission. In order to delineate the Ce 4*f* contributions, we have carefully subtracted the He I spectrum from the He II spectrum as shown in Fig. 3. The subtracted spectra shown in Fig. 3(a) represent three distinct features U, S, and K. The ground state of Ce 4*f* band can be expressed as a linear combination of $|f^0\rangle$ and $|f^1\rangle$ electronic configurations. $|f^0\rangle$ will have no contribution in the photoemission signal. Various photoemission final states generating from $|f^1\rangle$ initial state is shown schematically in Fig. 3(b). The feature U corresponds to the unscreened final state (ionization peak) and appears around 2 eV binding energy as found in various other Ce intermetallics.[20,21] This also explains the underestimation of the photoemission intensity around this energy region in the calculated spectrum shown in Fig. 2.

The features, S and K, correspond to the screened photoemission final states, $|f^1_{7/2}\underline{C}\rangle$ and $|f^1_{5/2}\underline{C}\rangle$, respectively ($\underline{C}$ represent a hole in the conduction band).[22] It is to note here that such features can appear due to magnetic Ce 4*f* states as well as the Kondo singlets formed via quantum entanglement of the 4*f* states with the conduction electronic states. Thus, it is not *a priori* possible to attribute these features to the Kondo resonance features. The most important characteristic of the Kondo effect is its temperature dependence as Kondo singlet forms at low temperatures.

We plot the Ce 4*f* high-resolution spectra collected at different temperatures in the lower panel of Fig. 3(a). Interestingly, the features S and K exhibit significant enhancement in intensity with the decrease in temperature with respect to the intensity of the ionization peak. *This is a unique demonstration of the emergence of Kondo resonance features gradually with the decrease in temperature and convincingly attributes the features S and K, to the Kondo effect. Here, the signature of Kondo resonance features are distinctly different from those due to the magnetic* 4*f* *contributions. Ironically, this interesting phenomenon is observed in a system,* Ce_2RhSi_3 *which lies at the peak of the Doniach's phase diagram exhibiting long-range order.*

Various core-level spectra collected at 10 K and 300 K are shown in Fig. 4 by dashed line and circles, respectively. The Si 2*s* spectra exhibit a sharp feature with an asymmetry at higher binding energy side typical of a metallic system.[23] A change in temperature appears to have negligible influence—the asymmetry at the high binding energy side is reduced by a small amount. Rh 3*d* spectra shown in Fig. 4(c) exhibit distinct spin-orbit split signals corresponding to $3d_{5/2}$ and

$3d_{3/2}$ at about 307 eV and 312 eV, respectively (spin-orbit splitting ~5 eV). The decrease in temperature leads to a small narrowing of the signal as shown in Fig. 4(d) by expanding the Rh $3d_{5/2}$ region. In order to estimate the change in line shape, we have broadened the 10 K spectra by a Gaussian (FWHM=500 meV). Clearly, the broadened spectra have larger width than the width of the 300 K spectra in both the cases. Thus, the change in linewidth is less than 500 meV and can be attributed to the thermal effects.

Ce $3d$ spectra are shown in Figs. 4(e) and 4(f). The $3d_{5/2}$ and $3d_{3/2}$ signals appear at about 884 and 902 eV binding energies. Each of the features are accompanied by two weaker signals at about 880 eV and 898 eV, respectively. These weak intensities at lower binding energies correspond to the well-screened $4f^2$ final state where the core hole is screened by an electron transferred from the conduction band.[11,24] The intense features correspond to the $4f^1$ final state. In order to visualize the temperature induced effect, the $3d_{5/2}$ signal is shown in an expanded scale in Fig. 4(f). Clearly, a decrease in temperature leads to a significant narrowing of the signal along with a sharp decrease in the high binding energy asymmetry. A Gaussian broadening employed similar to those for Rh and Si core levels does not have any influence indicating that such effect has a different origin.

For better visualization of the change in line shape, we have subtracted the 10 K spectrum from the room temperature one and shown by area plot in the Fig. 4(f). Clearly, the largest change appears at higher binding energy side. It is well known that the asymmetry in the core-level line shape usually appears due to the metallicity—Doniach-Šunjić line shape.[14,23] The decrease in asymmetry indicates partial localization of the conduction electrons via emergence of the narrow feature at ϵ_F—a signature of Kondo resonance, and thus, reveal a new way to probe the Kondo effect.

V. CONCLUSIONS

In summary, the high resolution and low temperature employed in this study enabled us to demonstrate the emergence of Kondo resonance features with the decrease in temperature. Interestingly, such features are observed in a system exhibiting long-range magnetic order that supports the views based on spin-density-wave scenario while approaching quantum criticality.

ACKNOWLEDGMENT

S.P. thanks the Council of Scientific and Industrial Research, Govt. of India for financial support.

*kbmaiti@tifr.res.in

[1] N. B. Brandt and V. V. Moshchalkov, Adv. Phys. **33**, 373 (1984).
[2] S. Doniach, Physica B **91**, 231 (1977).
[3] J. W. Allen, J. Phys. Soc. Jpn. **74**, 34 (2005).
[4] P. Gegenwart, Q. Si, and F. Steglich, Nat. Phys. **4**, 186 (2008).
[5] Q. Si, S. Rabello, K. Ingersent, and J. L. Smith, Nature (London) **413**, 804 (2001).
[6] A. J. Millis, Phys. Rev. B **48**, 7183 (1993).
[7] S. Patil, K. K. Iyer, K. Maiti, and E. V. Sampathkumaran, Phys. Rev. B **77**, 094443 (2008).
[8] B. Chevalier, P. Lejay, J. Etourneau, and P. Hagenmuller, Solid State Commun. **49**, 753 (1984).
[9] I. Das and E. V. Sampathkumaran, J. Magn. Magn. Mater. **137**, L239 (1994).
[10] N. Kase, T. Muranaka, and J. Akimitsu, J. Magn. Magn. Mater. **321**, 3380 (2009).
[11] M. Szlawska, D. Kaczorowski, A. Ślebarski, L. Gulay, and J. Stępień-Damm, Phys. Rev. B **79**, 134435 (2009).
[12] T. Nakano, K. Sengupta, S. Rayaprol, M. Hedo, Y. Uwatoko, and E. V. Sampathkumaran, J. Phys.: Condens. Matter **19**, 326205 (2007).
[13] P. Blaha, K. Schwarz, G. K. H. Madsen, D. Kvasnicka, and J. Luitz, *WIEN2k: An Augmented Plane Wave + Local Orbitals Program for Calculating Crystal Properties*, edited by K. Schwarz (Technische Universität Wien, Austria, 2001).
[14] M. Imada, A. fujimori, and Y. Tokura, Rev. Mod. Phys. **70**, 1039 (1998).
[15] D. D. Sarma, N. Shanthi, S. R. Barman, N. Hamada, H. Sawada, and K. Terakura, Phys. Rev. Lett. **75**, 1126 (1995); K. Maiti, Phys. Rev. B **73**, 235110 (2006); **73**, 115119 (2006); **77**, 212407 (2008).
[16] We have subtracted integral background from Al $K\alpha$ and He II spectra. Since the thermalized electrons lead to a large increase in background at low kinetic energies, we used a quadratic polynomial as a background function for He I spectrum as usually done.
[17] J. J. Yeh and I. Lindau, At. Data Nucl. Data Tables **32**, 1 (1985).
[18] Photoemission cross section of hybridized states may be different from those calculated using atomic wave functions in Ref. 17.
[19] S. Patil, S. K. Pandey, V. R. R. Medicherla, R. S. Singh, R. Bindu, E. V. Sampathkumaran, and K. Maiti, J. Phys.: Condens. Matter **22**, 255602 (2010).
[20] F. Patthey, W.-D. Schneider, Y. Baer, and B. Delley, Phys. Rev. Lett. **58**, 2810 (1987); F. Patthey, J. M. Imer, W.-D. Schneider, H. Beck, Y. Baer, and B. Delley, Phys. Rev. B **42**, 8864 (1990).
[21] Yu. Kucherenko, S. L. Molodtsov, A. N. Yaresko, and C. Laubschat, Phys. Rev. B **70**, 045105 (2004); C. Laubschat, S. Danzenbächer, D. V. Vyalikh, S. L. Molodtsov, and Yu. Kucherenko, Phys. Status Solidi B **246**, 1450 (2009).
[22] D. Ehm, S. Hüfner, F. Reinert, J. Kroha, P. Wölfle, O. Stockert, C. Geibel, and H. v. Löhneysen, Phys. Rev. B **76**, 045117 (2007); M. Klein, A. Nuber, F. Reinert, J. Kroha, O. Stockert, and H. v. Löhneysen, Phys. Rev. Lett. **101**, 266404 (2008).
[23] S. Doniach and M. Šunjić, J. Phys. C **3**, 285 (1970); R. S. Singh and K. Maiti, Solid State Commun. **140**, 188 (2006).
[24] O. Gunnarsson and K. Schönhammer, Phys. Rev. B **28**, 4315 (1983); A. Kakizaki, A. Harasawa, T. Ishii, T. Kashiwakura, A. Kamata, and S. Kunii, J. Phys. Soc. Jpn. **64**, 302 (1995).